Mechanochemistry Hot Paper

How to cite: *Angew. Chem. Int. Ed.* **2021**, *60*, 15365–15370
International Edition: doi.org/10.1002/anie.202100675
German Edition: doi.org/10.1002/ange.202100675

Cucurbituril-Encapsulating Metal–Organic Framework via Mechanochemistry: Adsorbents with Enhanced Performance

*Jun Liang, Vasily Gvilava, Christian Jansen, Secil Öztürk, Alex Spieß, Jingxiang Lin, Shanghua Xing, Yangyang Sun, Hao Wang, and Christoph Janiak**

Abstract: *The first examples of monolithic crystalline host–guest hybrid materials are described. The reaction of 1,3,5-benzenetricarboxylic acid (H_3BTC) and $Fe(NO_3)_3{\cdot}9H_2O$ in the presence of decamethylcucurbit[5]uril ammonium chloride ($MC5{\cdot}2NH_4Cl{\cdot}4H_2O$) directly affords MC5@MIL-100(Fe) hybrid monoliths featuring hierarchical micro-, meso- and macropores. Particularly, this "bottle-around-ship" synthesis and one-pot shaping are facilitated by a newly discovered Fe-MC5 flowing gel formed by mechanochemistry. The designed MC5@MIL-100(Fe) hybrid material with MC5 as active domains shows enhanced CH_4 and lead(II) uptake performance, and selective capture of lead(II) cations at low concentrations. This shows that host–guest hybrid materials can exhibit synergic properties that out-perform materials based on individual components.*

The past three decades has witnessed the revolutionary impact of cage-like molecules,[1] such as cyclodextrin,[2] calixarene,[3] pillarene,[4] and imine cages on separation technology,[5] since these functional molecules have both adsorption sites/cavity and potential to fabricate advanced hybrid systems. In particular, cucurbit[*n*]urils (CB[*n*]s, $n = 5$–10) are easily synthesized by the condensation of formaldehyde and glycolurils.[6] Due to their rich functional groups and symmetrical structures with hydrophilic portals and hydrophobic pores, CB[*n*] have found various applications including molecular recognition and assembly,[7] switches,[8] catalysis,[9] and separations.[10] Yet, the designed synthesis of CB-based porous solids remains an ongoing challenge due to their relatively inert structures and tendency to aggregate.[6b,7b] As one of the earliest discovered CB[*n*]s, decamethylcucurbit-[5]uril (MC5) has a rigid cage with carbonyl groups on each portal and a portal size of 2.5 Å (Scheme 1). Although MC5 shows some attractive features including good water-solubility and selective binding toward Pb^{II}, its application is limited by its nonporous solid-state structure.[11] Encapsulation of CB in the pores of a host matrix could circumvent this problem and, thus, afford the opportunity to achieve functional host–guest hybrid materials.[12]

Metal–organic frameworks (MOFs) with tunable structures, well-defined pores and high surface areas are demonstrated to be perfect host frameworks for various guests (e.g. polyoxometalates, nanoparticles, semiconductors, polymers, poly(ionic liquid)s and enzymes).[13] Consequently, advanced host–guest hybrid materials have been obtained by using a variety of synthetic methodologies, such as impregnation,[14] ion exchange,[15] "ship-in-a-bottle",[16] and chemical vapor deposition (CVD),[17] impacting technologies from gas separation to catalysis. Despite all the progress made in the fabrication of these MOF-based host–guest hybrid materials, it's challenging to achieve designed fabrication of cage-like or

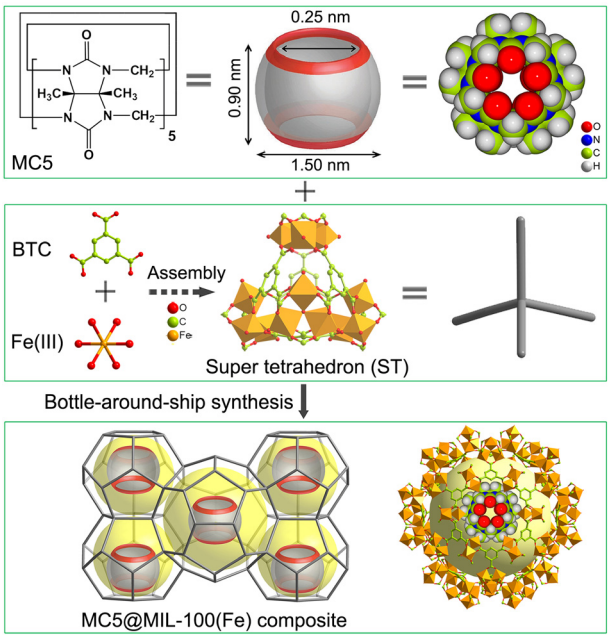

Scheme 1. Encapsulation of decamethylcucurbit[5]uril (MC5) cages into the in situ formed MIL-100(Fe) via a "bottle-around-ship" synthesis. Hydrogen atoms are omitted for clarity.

[*] Dr. J. Liang, Dr. S. Xing, Dr. H. Wang, Prof. Dr. C. Janiak
Hoffmann Institute of Advanced Materials, Shenzhen Polytechnic
7098 Liuxian Blvd, Nanshan District, Shenzhen 518055 (China)
Dr. J. Liang, V. Gvilava, C. Jansen, S. Öztürk, A. Spieß, Dr. S. Xing, Y. Sun, Prof. Dr. C. Janiak
Institut für Anorganische Chemie und Strukturchemie, Heinrich-Heine-Universität Düsseldorf
40204 Düsseldorf (Germany)
E-mail: janiak@uni-duesseldorf.de
Dr. J. Lin
The School of Ocean Science and Biochemistry Engineering, Fuqing Branch of Fujian Normal University
Fuqing 350300 (China)
Supporting information and the ORCID identification number(s) for the author(s) of this article can be found under: https://doi.org/10.1002/anie.202100675.

macrocyclic molecules/MOF hybrids.[18] Up to now, a few macrocycle-encapsulating MOF hybrid materials have been reported.[13g,19] For example, porphyrins have been successfully encapsulated into metal–organic materials (MOMs) to obtain porph@MOM hybrids as artificial enzymes.[19c] We continued our quest toward fabrication and shaping of functional CB@MOF materials via facile approaches. The challenge lies in the choice of CB molecules with good solubility,[6b] and the encapsulation of CB molecules with retaining active domains.[20] Particularly, MC5 and CB[*n*] (*n* = 5, 7) have good water solubility, providing the potential to be hydrogelators.[21] We proposed that if soluble CB cages and MOF precursors can be well mixed in a condensed phase, such as a gel via mechanochemistry,[22] then the encapsulation of CB into the pores of in situ formed MOF can be achieved via bottle-around-ship synthesis (Scheme 1), giving CB@MOF materials for exploring CB related properties.

Here we report for the first time, a "bottle-around-ship" approach to prepare MC5@MIL-100(Fe) hybrid monoliths with hierarchical pores, which is facilitated by an unprecedented Fe-MC5 flowing gel formed by mechanochemistry (Figure 1 a). The MC5@MIL-100(Fe) composites show enhanced performance over its components for CH_4 uptake and Pb^{II} removal at low concentrations.

MIL-100(Fe), formed through the assembly of BTC anions and iron(III) cations,[23] served as a host as its topology affords two kinds of mesoporous cages (25 Å and 29 Å) to encapsulate MC5 molecules with an outer diameter of 15 Å and a height of 9 Å (Scheme 1, Figure S2 in the Supporting Information). Briefly, individually pre-ground H_3BTC crystallites, MC5·2NH_4Cl·4H_2O and $Fe(NO_3)_3$·9H_2O (Figure S3–S5) were ground to form a H_3BTC/Fe-MC5 flowing gel at room temperature under relative humidity over 40% (see Video S1). Then, heating the gel in a Teflon autoclave for five hours afforded the hybrids designated as MC5@MIL-100(Fe)-W (W = 12, 20, 23), where W represents the weight percentage of imbedded MC5 in the material based on elemental analysis (See Supporting Information). We noticed that amorphous Fe-BTC gel and aerogels can be obtained via sol-gel approaches as reported by James and others.[24]

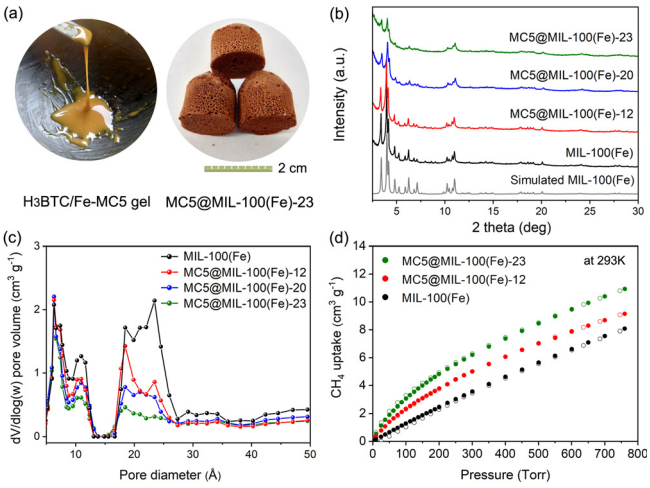

Figure 1. (a) H_3BTC/Fe-MC5 flowing gel and monoliths on a macroscopic scale, (b) PXRD patterns, (c) pore size distributions based on N_2 sorption isotherms (Figure S20) at 77 K of MIL-100(Fe) and MC5@MIL-100(Fe)-W (weight percentage W = 12, 20, 23), and (d) CH_4 sorption isotherms of MIL-100(Fe) and MC5@MIL-100(Fe)-12, 23.

MC5@MIL-100(Fe) hybrids were obtained as monoliths (Figure 1 a, and S6), which were robust in hot water (80 °C) and ethanol (65 °C), and had macropores of 100–300 μm (Figure S7–S8), thus facilitating activation and solvent exchange with retention of shape. In contrast, MIL-100(Fe) collapsed into particles in water. Powder X-ray diffraction (PXRD) patterns of MC5@MIL-100(Fe) hybrids matched that of MIL-100(Fe) (Figure 1 b), confirming the construction of the intended framework.[23] The presence of MC5 in MIL-100(Fe) was supported by Fourier Transform infrared spectroscopy (FT-IR), which shows the characteristic vibration bands of uncoordinated MC5 and MIL-100(Fe), suggesting MC5 as guest molecules (Figure S9). Incubation of composites in an aqueous solution of K^+ ions showed no release of MC5, as indicated by ^{1}H NMR studies of the solution (Figure S10). Dissolving hybrids under strongly basic solutions permitted the estimation of the molar ratios of BTC to MC5 in MC5@MIL-100(Fe) by ^{1}H NMR, which was consistent with the elemental analysis for each sample (Figure S11–S13, Table S1). These findings support the encapsulation of uncoordinated MC5 cages and the absence of MC5 leaching, mainly due to the smaller size of the MOF window apertures than the MC5 cage size. Compared with MIL-100(Fe), more closely stacked and arrayed crystallites were observed in MC5@MIL-100(Fe)-20,23 based on scanning electron microscopy (SEM) analyses (Figure S14). Thus, Fe-MC5 gel could facilitate the fusion of MOF crystallites to give brittle MC5@MIL-100(Fe) monoliths with macropores (Figure S15-S16). In addition, energy dispersive X-ray (EDX) spectroscopy element mapping showed a homogeneous distribution of the Fe, N, O elements in MC5@MIL-100(Fe)-23 (Figure S17). Neither PXRD patterns nor transition electron microscopy (TEM) analysis gave an indication for the formation of iron oxide in MC5@MIL-100(Fe)-23 (Figure S18). Thermogravimetric analyses (TGA) showed that MC5@MIL-100(Fe) hybrids can be stable up to 280 °C under air (Figure S19).

The porosities of all materials were investigated by nitrogen sorption at 77 K, showing the Type-Ib isotherms with H4 loop (Figure S20). The Brunauer-Emmett-Teller (BET) surface areas of MIL-100(Fe), and MC5@MIL-100(Fe)-12,20,23 was found to be 1745, 1254, 1140, and 895 $m^2 g^{-1}$, respectively (Table S2). Compared with MIL-100(Fe), the pore volumes and surface areas of the hybrid materials gradually decreased due to the occupation of the mesopores of MIL-100(Fe) with increasing amount of MC5 molecules. The drop in porosity with incorporation of MC5 is not linear but most pronounced from neat MIL-100 to MC5@MIL-100(Fe)-12 (Table S2). This is reasoned by the "bottle-around-ship synthesis", where the MC5 molecules decrease the porosity by both the occupation of mesopores and affecting the formation process of the MIL-100 frameworks in the hybrids. Thereby, some pores in the hybrid frameworks may be blocked and some amorphous phase develops in MC5@MIL-100(Fe) as suggested by their PXRD patterns (Figure 1 b). The chemical stability of MC5@MIL-100(Fe)-23

in various solvents was evaluated by PXRD peaks and BET surface areas. After soaking in ethanol, acetone, acetonitrile and tetrahydrofuran for 24 hours, MC5@MIL-100(Fe)-23 retained its crystallinity and around 80% of its surface areas (Figure S21).

Moreover, the macropore size distribution analyses (Figure S16) proved the hierarchical porous structures of MC5@MIL-100(Fe) with pore size distribution from nanometers (4–10 nm) to micrometers (4–100 μm). Thus, the Type H4 hysteresis loop in isotherms can be attributed to the existence of mesopores (>2 nm) and aggregated crystals.[25] The multiple roles of MC5 molecules to occupy mesopores and to induce macropores in hybrid materials were further suggested by the pore features of monolithic MIL-100(Fe) (Figure S22-S23). $_{mono}$MIL-100(Fe) can be formed by mechanochemical synthesis with the addition of NH_4Cl instead of MC5·2 NH_4Cl·4 H_2O and has similar BET surface areas (1829 $m^2 g^{-1}$) and pore size distribution with MIL-100(Fe) (Figure S23, Supporting Information). The fraction of macropores and their upper value is higher in MC5@MIL-100(Fe) than in $_{mono}$MIL-100(Fe). This can be understood by the action of the MC5 molecules during the "bottle-around-ship synthesis" affecting the formation process of the MIL-100 frameworks and the hybrid monoliths.

Despite the decreased porosities, MC5@MIL-100(Fe)-12, 23 exhibited similar CO_2 uptakes and enhanced CH_4 adsorption performance over MIL-100(Fe) probably due to the interactions between CH_4 and MC5 (Figure 1d, Table S2, Figure S26–S28).[26] Indeed, pure MC5 adsorbent showed steeper CH_4 adsorption curves but required more time to reach the thermodynamic equilibrium at each data point. This indicates slower adsorption kinetics than those of MC5@MIL-100(Fe) and MIL-100(Fe) due to the nonporous structure of MC5 solid (Figure S29). To investigate the possible binding sites for CH_4 on MC5, DFT-D3 (dispersion-corrected DFT) calculations were conducted. Gas-phase geometry optimization of CH_4 with MC5 yields three different possibilities (CH_4^I, CH_4^{II} and CH_4^{III}) for CH_4 binding (Figure S30, Table S3). Specifically, CH_4 can be located around the outer surface (CH_4^I, CH_4^{II}) and in the cavity of MC5 cage (CH_4^{III}). CH_4 molecules are mainly adsorbed through the C···H dispersive interactions, $O^{\delta-}\cdots H^{\delta+}$ and $N^{\delta-}\cdots H^{\delta+}$ electrostatic interactions (Table S3). DFT calculated static binding energies of CH_4 molecules on MC5 are −7, −11.8 and −44 kJ mol^{-1} for CH_4^I, CH_4^{II} and CH_4^{III}, respectively, suggesting the weak to moderate interactions between CH_4 molecules and MC5. Considering that the kinetic diameter (3.8 Å) of CH_4 is larger than the portal size (2.5 Å) of MC5, outer surface interactions could be predominant in the hybrid materials under 1 bar. Moreover, the CH_4 uptake of MC5@MIL-100(Fe)-23 reaches 65.4 $cm^3 g^{-1}$ at 44.2 bar and 298 K (Figure S31), which was 29% of the uptake at 44.9 bar of $_{mono}$HKUST-1 which was reported to have the highest v/v methane uptake 259 cm^3 (STP) cm^{-3}.[27]

We propose that the Fe-MC5 gel formation is initiated by the chloride ions from MC5·2 NH_4Cl·4 H_2O, which react with the iron centers in $Fe(NO_3)_3$·9 H_2O to form iron-chloride species under shear force,[28] providing multiple interactions including hydrogen-bonds, weak coordination and ionic

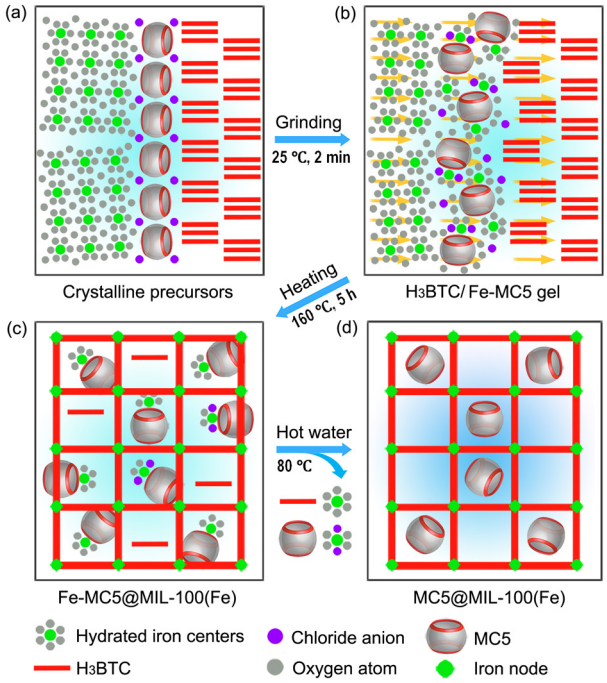

Figure 2. The H_3BTC/Fe-MC5 flowing gel formation and fabrication of MC5@MIL-100(Fe). (a) Snapshot of the interfaces among $Fe(NO_3)_3$·9 H_2O, MC5·2 NH_4Cl·4 H_2O and H_3BTC; nitrate and ammonium ions are not shown; (b) chloride ions from MC5·2NH_4Cl·4 H_2O attack iron centers in $Fe(NO_3)_3$·9 H_2O to form iron-chloride species in H_3BTC/Fe-MC5 gel; (c) heating the gel in a Teflon autoclave leads to Fe-MC5@MIL-100(Fe); (d) hot water triggered activation to give porous MC5@MIL-100(Fe).

interactions with MC5 molecules (Figure 2, and S33–S34). Moreover, the Fe-MC5 gel formation process was not affected by the presence of H_3BTC crystallites due to their poor water solubility (Figure 1a, and S35–S36). As a result, H_3BTC crystallites can be well dispersed in the Fe-MC5 flowing gel within a few minutes under grinding to provide fluid processible precursors for direct fabrication of monolithic MC5@MIL-100 composites. To confirm that the formation of iron-chloride species takes place during grinding and gel formation, control experiments were conducted (Figure S37–S40, Table S4, Supporting Information). Notably, $Fe(NO_3)_3$·9 H_2O and NH_4Cl rapidly reacted under shear force to afford a yellow gel termed Fe-Cl with a molar ratio of Fe:Cl at 6:1 (Supporting Video S3).

Besides, a non-gel slurry containing the known phase $(NH_4)_2[FeCl_5(OH_2)]$ was formed with a Fe-$(NO_3)_3$·9 H_2O:NH_4Cl molar ratio of 6:18 based on PXRD and Raman analysis (Figure S38–S40, Supporting Information). These results support our proposal and indicate the important role of Fe:Cl molar ratio for successful gel formation via mechanochemistry. This fundamental understanding of the gel formation may guide monolithic MOF design and function integration to achieve enhanced properties.

We measured the PXRD and IR spectra data of the H_3BTC/Fe-MC5 gel to monitor the phase and interaction changes during the fabrication of MC5@MIL-100(Fe)-23

(Figure S41–S44). As shown in Figure S41, H_3BTC turns amorphous in the presence of the Fe-MC5 gel at elevated temperature (from 60 °C up to 160 °C), probably by dissolution and reaction with iron centers (Figure S43). At 160 °C for up to 60 min, clearly identifiable phase of intended MIL-100(Fe) framework has formed (Figure S44). Coordination of Fe to MC5 probably facilitated the MC5-encapsulation as the Fe centers became constituent parts of MIL-100(Fe) (Figure 2c,d).

MC5 was reported to show high capture of Pb^{II} in an aqueous solution.[11b] To illustrate the sorption capabilities of MC5@MIL-100(Fe)-23 with MC5 as active component (Figure 3a), we investigated the Pb^{II} capture behavior of solid MC5@MIL-100(Fe)-23 in comparison to MIL-100(Fe) and solid MC5·2 NH_4Cl·4 H_2O at a concentration of 1 mg L^{-1} (see the Supporting Information). We observed faster uptake kinetics (0.239 versus 0.094 g mg^{-1} min^{-1}) and higher removal efficiency (99.7 % versus 53 %) for Pb^{II} by MC5@MIL-100(Fe)-23 than by MIL-100(Fe) (Figure S47, Table S5). In contrast, a low removal efficiency (≈8 %) was obtained by the equal amount of MC5·2 NH_4Cl·4 H_2O solid due to its nonporous structure. The mechanistic analyses of the adsorption kinetics indicated that chemisorption, that is, the formation of chemical bonds and not intraparticle diffusion was the dominant adsorption rate limiting step for MC5@MIL-100(Fe)-23 and MIL-100(Fe) (Figure S48–S49, Table S5). The calculated kinetic rate constant k_2 of MC5@MIL-100(Fe)-23 was 0.239 g mg^{-1} min^{-1}, which is significantly higher than many other Pb^{II} adsorbents.[29] Moreover, the adsorption isotherms for both adsorbents (Figure 3b, and S50) showed that a noticeably higher uptake capacity and removal efficiency could be achieved by MC5@MIL-100(Fe)-23 at Pb^{II} initial concentrations from 1 mg L^{-1} to 100 mg L^{-1} at pH 6.0. The experimental saturated uptake amount was 29 mg g^{-1} (Figure 3b and S51-S52 and Table S6). These findings indicate the significant role of MC5 in the composite for enhanced Pb^{II} removal. The framework of MC5@MIL-100(Fe)-23 after Pb^{II} capture is largely retained based on PXRD and N_2-sorption/BET analyses (Figure S53, Supporting Information).

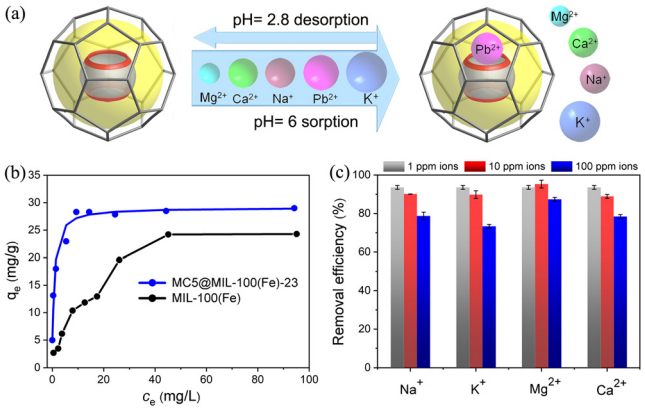

Figure 3. (a) The selective capture of lead(II) by MC5@MIL-100(Fe)-23 among other common cations in water. (b) Pb^{II} adsorption isotherms by MC5@MIL-100(Fe)-23 and MIL-100(Fe). (c) The effects of coexisting ions on the removal efficiency of Pb^{II} at an initial concentration of 1 mg L^{-1} (1 ppm) by MC5@MIL-100(Fe)-23.

To shed light on the Pb^{II} sorption sites in MC5@MIL-100(Fe)-23, IR spectra after Pb^{II} uptake, also in the presence of mineral ions, showed that the vibrations of the carbonyl groups of MC5 were red-shifted from 1749 cm^{-1} to 1730 cm^{-1} while increasing the concentration of Pb^{II} solution from 1 ppm to 15 ppm (Figure S54–S58), which was attributed to the coordination interactions with Pb^{II}. This was supported by the red-shifted peaks of carbonyl groups in Pb-MC5 complexes (Figure S55). The coordination of Pb^{II} was supported by a high resolution Pb 4f X-ray photoelectron spectral (XPS) analysis of Pb-MC5@MIL-100(Fe)-23 (Figure S59). Compared with Pb^{II} binding energies of $Pb(NO_3)_2$ centered at 139.6 eV and 144.5 eV for Pb $4f_{7/2}$ and $4f_{5/2}$, a shift of 0.3 eV to lower binding energies at 139.3 eV and 144.2 eV was observed, suggesting modest interactions between Pb^{II} and MC5.[30] Moreover, MC5@MIL-100(Fe)-23 could be recycled by Pb desorption with dilute nitric acid and exhibited almost unchanged removal efficiency over three runs (Figure S60).

MC5@MIL-100(Fe)-23 could also efficiently remove Pb^{II} at a low concentration in the presence of various amounts of mineral ions (Na^+, K^+, Mg^{2+}, and Ca^{2+}). As shown in Figure 3c, 94 %, 89 % or 73 % Pb^{II} could be removed in the presence of 1-fold, 10-fold or 100-fold amount of disturbing ions. For a mixed solution containing equal amount of mineral ions and Pb^{II} at 10 ppm, a removal efficiency of 67 % (33 mg g^{-1}) was still obtained, confirming the selective capture capability of MC5@MIL-100(Fe)-23 with MC5 as recognition domain toward Pb^{II}.

In conclusion, we have successfully used a newly discovered Fe-MC5 flowing gel to fabricate MC5@MIL-100(Fe) hybrid materials via facile mechanochemical synthesis. The interplay of both chemistry and mechanics leads to the formation of hygroscopic iron-chloride species, which is critical for the formation of MC5-Fe gel. Compared to MIL-100(Fe) and MC5·2 NH_4Cl·4 H_2O alone, MC5@MIL-100(Fe)-23 with MC5 molecules as active domains exhibits enhanced performance due to the encapsulation of MC5 molecules in the porous matrix, which efficiently avoided the drawback of MC5 solid with "nonporous" structure and the lack of functional groups in MIL-100(Fe) framework. This work opens up the novel possibility of designing task-specific porous host–guest hybrid materials on a macroscopic scale based on mechanochemical synthesis. Work is under way to expand this approach to numerous other types of cages and MOFs, which can permit access to new functional materials for sorption, catalysis, etc.

Acknowledgements

J.L. acknowledges financial support of NSFC (22001178) and support from the Hoffmann Institute of Advanced Materials (HIAM), Shenzhen Polytechnic. We thank Dr. Raphael Wiedey, Dr. Alexa Schmitz, Lars Rademacher, Saskia Menzel, Dennis Woschko and Stephanie Bügel at Heinrich-Heine-Universität Düsseldorf for their help. Open access funding enabled and organized by Projekt DEAL.

Conflict of interest

The authors declare no conflict of interest.

Keywords: cucurbituril · host–guest hybrid · lead(II) · mechanochemistry · metal–organic framework

[1] a) T. Hasell, A. I. Cooper, *Nat. Rev. Mater.* **2016**, *1*, 16053; b) Z. Liu, S. K. M. Nalluri, J. F. Stoddart, *Chem. Soc. Rev.* **2017**, *46*, 2459 – 2478.

[2] a) G. Crini, *Chem. Rev.* **2014**, *114*, 10940 – 10975; b) K. J. Hartlieb, J. M. Holcroft, P. Z. Moghadam, N. A. Vermeulen, M. M. Algaradah, M. S. Nassar, Y. Y. Botros, R. Q. Snurr, J. F. Stoddart, *J. Am. Chem. Soc.* **2016**, *138*, 2292 – 2301.

[3] P. K. Thallapally, B. P. McGrail, S. J. Dalgarno, H. T. Schaef, J. Tian, J. L. Atwood, *Nat. Mater.* **2008**, *7*, 146 – 150.

[4] a) N. Song, T. Kakuta, T.-a. Yamagishi, Y.-W. Yang, T. Ogoshi, *Chem* **2018**, *4*, 2029 – 2053; b) W. Xue, P. Y. Zavalij, L. Isaacs, *Angew. Chem. Int. Ed.* **2020**, *59*, 13313 – 13319; *Angew. Chem.* **2020**, *132*, 13415 – 13421; c) J. R. Wu, B. Li, Y. W. Yang, *Angew. Chem. Int. Ed.* **2020**, *59*, 2251 – 2255; *Angew. Chem.* **2020**, *132*, 2271 – 2275.

[5] a) M. Liu, L. Zhang, M. A. Little, V. Kapil, M. Ceriotti, S. Yang, L. Ding, D. L. Holden, R. Balderas-Xicohténcatl, D. He, R. Clowes, S. Y. Chong, G. Schütz, L. Chen, M. Hirscher, A. I. Cooper, *Science* **2019**, *366*, 613 – 620; b) Y. Liu, W. Zhao, C.-H. Chen, A. H. Flood, *Science* **2019**, *365*, 159 – 161; c) T. Mitra, K. E. Jelfs, M. Schmidtmann, A. Ahmed, S. Y. Chong, D. J. Adams, A. I. Cooper, *Nat. Chem.* **2013**, *5*, 276 – 281.

[6] a) K. I. Assaf, W. M. Nau, *Chem. Soc. Rev.* **2015**, *44*, 394 – 418; b) J. Lagona, P. Mukhopadhyay, S. Chakrabarti, L. Isaacs, *Angew. Chem. Int. Ed.* **2005**, *44*, 4844 – 4870; *Angew. Chem.* **2005**, *117*, 4922 – 4949; c) H. Cong, X. L. Ni, X. Xiao, Y. Huang, Q. J. Zhu, S. F. Xue, Z. Tao, L. F. Lindoy, G. Wei, *Org. Biomol. Chem.* **2016**, *14*, 4335 – 4364.

[7] a) S. J. Barrow, S. Kasera, M. J. Rowland, J. del Barrio, O. A. Scherman, *Chem. Rev.* **2015**, *115*, 12320 – 12406; b) R. N. Dsouza, U. Pischel, W. M. Nau, *Chem. Rev.* **2011**, *111*, 7941 – 7980; c) J. Murray, K. Kim, T. Ogoshi, W. Yao, B. C. Gibb, *Chem. Soc. Rev.* **2017**, *46*, 2479 – 2496; d) X.-L. Ni, X. Xiao, H. Cong, L.-L. Liang, K. Cheng, X.-J. Cheng, N.-N. Ji, Q.-J. Zhu, S.-F. Xue, Z. Tao, *Chem. Soc. Rev.* **2013**, *42*, 9480 – 9508.

[8] Y. Ahn, Y. Jang, N. Selvapalam, G. Yun, K. Kim, *Angew. Chem. Int. Ed.* **2013**, *52*, 3140 – 3144; *Angew. Chem.* **2013**, *125*, 3222 – 3226.

[9] a) S. Funk, J. Schatz, *J. Inclusion Phenom. Macrocyclic Chem.* **2020**, *96*, 1 – 27; b) H. You, D. Wu, Z. Chen, F. Sun, H. Zhang, Z. Chen, M. Cao, W. Zhuang, R. Cao, *ACS Energy Lett.* **2019**, *4*, 1301 – 1307; c) S. Zhang, M. Cao, R. Cao, *ACS Sustainable Chem. Eng.* **2020**, *8*, 9217 – 9225.

[10] a) Y. Huang, R. H. Gao, M. Liu, L. X. Chen, X. L. Ni, X. Xiao, H. Cong, Q. J. Zhu, K. Chen, Z. Tao, *Angew. Chem. Int. Ed.* **2021**, https://doi.org/10.1002/anie.202002666; *Angew. Chem.* **2021**, https://doi.org/10.1002/ange.202002666; b) K. Chen, Y. S. Kang, Y. Zhao, J. M. Yang, Y. Lu, W. Y. Sun, *J. Am. Chem. Soc.* **2014**, *136*, 16744 – 16747; c) H. Kim, Y. Kim, M. Yoon, S. Lim, S. M. Park, G. Seo, K. Kim, *J. Am. Chem. Soc.* **2010**, *132*, 12200 – 12202.

[11] a) A. Flinn, G. C. Hough, J. F. Stoddart, D. J. Williams, *Angew. Chem. Int. Ed. Engl.* **1992**, *31*, 1475 – 1477; *Angew. Chem.* **1992**, *104*, 1550 – 1551; b) X. X. Zhang, K. E. Krakowiak, G. Xue, J. S. Bradshaw, R. M. Izatt, *Ind. Eng. Chem. Res.* **2000**, *39*, 3516 – 3520; c) Y. Miyahara, K. Abe, T. Inazu, *Angew. Chem. Int. Ed.* **2002**, *41*, 3020 – 3023; *Angew. Chem.* **2002**, *114*, 3146 – 3149.

[12] J. Liang, A. Nuhnen, S. Millan, H. Breitzke, V. Gvilava, G. Buntkowsky, C. Janiak, *Angew. Chem. Int. Ed.* **2020**, *59*, 6068 – 6073; *Angew. Chem.* **2020**, *132*, 6124 – 6129.

[13] a) G. Maurin, C. Serre, A. Cooper, G. Férey, *Chem. Soc. Rev.* **2017**, *46*, 3104 – 3107; b) H. Furukawa, K. E. Cordova, M. O'Keeffe, O. M. Yaghi, *Science* **2013**, *341*, 1230444; c) L. Chen, R. Luque, Y. Li, *Chem. Soc. Rev.* **2017**, *46*, 4614 – 4630; d) J. Juan-Alcañiz, J. Gascon, F. Kapteijn, *J. Mater. Chem.* **2012**, *22*, 10102 – 10118; e) Q. Yang, Q. Xu, H.-L. Jiang, *Chem. Soc. Rev.* **2017**, *46*, 4774 – 4808; f) T. Kitao, Y. Zhang, S. Kitagawa, B. Wang, T. Uemura, *Chem. Soc. Rev.* **2017**, *46*, 3108 – 3133; g) I. Cota, F. Fernandez Martinez, *Coord. Chem. Rev.* **2017**, *351*, 189 – 204; h) S. Huang, X. Kou, J. Shen, G. Chen, G. Ouyang, *Angew. Chem. Int. Ed.* **2020**, *59*, 8786 – 8798; *Angew. Chem.* **2020**, *132*, 8868 – 8881; i) G. Huang, L. Yang, Q. Yin, Z.-B. Fang, X.-J. Hu, A.-A. Zhang, J. Jiang, T.-F. Liu, R. Cao, *Angew. Chem. Int. Ed.* **2020**, *59*, 4385; *Angew. Chem.* **2020**, *132*, 4415; j) L. Li, J.-D. Yi, Z.-B. Fang, X.-S. Wang, N. Liu, Y.-N. Chen, T.-F. Liu, R. Cao, *Chem. Mater.* **2019**, *31*, 7584 – 7589.

[14] a) C. W. Kung, K. Otake, C. T. Buru, S. Goswami, Y. Cui, J. T. Hupp, A. M. Spokoyny, O. K. Farha, *J. Am. Chem. Soc.* **2018**, *140*, 3871 – 3875; b) J. Yu, Y. Cui, C. Wu, Y. Yang, Z. Wang, M. O'Keeffe, B. Chen, G. Qian, *Angew. Chem. Int. Ed.* **2012**, *51*, 10542 – 10545; *Angew. Chem.* **2012**, *124*, 10694 – 10697.

[15] D. T. Genna, A. G. Wong-Foy, A. J. Matzger, M. S. Sanford, *J. Am. Chem. Soc.* **2013**, *135*, 10586 – 10589.

[16] a) B. Li, Y. Zhang, D. Ma, T. Ma, Z. Shi, S. Ma, *J. Am. Chem. Soc.* **2014**, *136*, 1202 – 1205; b) X. Qiu, W. Zhong, C. Bai, Y. J. Li, *J. Am. Chem. Soc.* **2016**, *138*, 1138 – 1141.

[17] S. Hermes, F. Schröder, S. Amirjalayer, R. Schmid, R. A. Fischer, *J. Mater. Chem.* **2006**, *16*, 2464 – 2472.

[18] a) H. Zhang, R. Zou, Y. Zhao, *Coord. Chem. Rev.* **2015**, *292*, 74 – 90; b) U. Jeong, N. A. Dogan, M. Garai, T. S. Nguyen, J. F. Stoddart, C. T. Yavuz, *J. Am. Chem. Soc.* **2019**, *141*, 12182 – 12186; c) L. L. Tan, H. Li, Y. C. Qiu, D. X. Chen, X. Wang, R. Y. Pan, Y. Wang, S. X. Zhang, B. Wang, Y. W. Yang, *Chem. Sci.* **2015**, *6*, 1640 – 1644.

[19] a) M. H. Alkordi, Y. Liu, R. W. Larsen, J. F. Eubank, M. Eddaoudi, *J. Am. Chem. Soc.* **2008**, *130*, 12639 – 12641; b) Z. Zhang, L. Zhang, L. Wojtas, P. Nugent, M. Eddaoudi, M. J. Zaworotko, *J. Am. Chem. Soc.* **2012**, *134*, 924 – 927; c) R. W. Larsen, L. Wojtas, J. Perman, R. L. Musselman, M. J. Zaworotko, C. M. Vetromile, *J. Am. Chem. Soc.* **2011**, *133*, 10356 – 10359.

[20] Q. W. Li, W. Y. Zhang, O. S. Miljanic, C. H. Sue, Y. L. Zhao, L. H. Liu, C. B. Knobler, J. F. Stoddart, O. M. Yaghi, *Science* **2009**, *325*, 855 – 859.

[21] I. Hwang, W. S. Jeon, H. J. Kim, D. Kim, H. Kim, N. Selvapalam, N. Fujita, S. Shinkai, K. Kim, *Angew. Chem. Int. Ed.* **2007**, *46*, 210 – 213; *Angew. Chem.* **2007**, *119*, 214 – 217.

[22] a) A. E. Danks, S. R. Hall, Z. Schnepp, *Mater. Horiz.* **2016**, *3*, 91 – 112; b) K. Sumida, K. Liang, J. Reboul, I. A. Ibarra, S. Furukawa, P. Falcaro, *Chem. Mater.* **2017**, *29*, 2626 – 2645; c) S. L. James, C. J. Adams, C. Bolm, D. Braga, P. Collier, T. Friščić, F. Grepioni, K. D. Harris, G. Hyett, W. Jones, A. Krebs, J. Mack, L. Maini, A. G. Orpen, I. P. Parkin, W. C. Shearouse, J. W. Steed, D. C. Waddell, *Chem. Soc. Rev.* **2012**, *41*, 413 – 447.

[23] P. Horcajada, S. Surblé, C. Serre, D. Y. Hong, Y. K. Seo, J. S. Chang, J. M. Grenèche, I. Margiolaki, G. Férey, *Chem. Commun.* **2007**, 2820 – 2822.

[24] a) Q. Wei, S. L. James, *Chem. Commun.* **2005**, 1555 – 1556; b) M. R. Lohe, M. Rose, S. Kaskel, *Chem. Commun.* **2009**, 6056 – 6058; c) J. Zhang, C.-Y. Su, *Coord. Chem. Rev.* **2013**, *257*, 1373 – 1408.

[25] M. Thommes, K. Kaneko, A. V. Neimark, J. P. Olivier, F. Rodriguez-Reinoso, J. Rouquerol, K. S. W. Sing, *Pure Appl. Chem.* **2015**, *87*, 1051 – 1069.

[26] Miyahara and co-workers reported that CO_2 (3.30 Å kinetic diameter) was adsorbed and desorbed repeatedly by neat MC5 powders, while CH_4 (3.80 Å kinetic diameter) was not adsorbed significantly in the solid state, but could be encapsulated into neat MC5 by heating in aqueous solution.[11c] Thus, synergistic adsorption sites of robust MC5@MOF hybrid might be available for but not limited to CO_2, CH_4, N_2O and NO.
[27] T. Tian, Z. Zeng, D. Vulpe, M. E. Casco, G. Divitini, P. A. Midgley, J. Silvestre-Albero, J.-C. Tan, P. Z. Moghadam, D. Fairen-Jimenez, *Nat. Mater.* **2018**, *17*, 174 – 179.
[28] S. A. Cotton, *J. Coord. Chem.* **2018**, *71*, 3415 – 3443.
[29] C. Yu, X. Han, Z. Shao, L. Liu, H. Hou, *Cryst. Growth Des.* **2018**, *18*, 1474 – 1482.
[30] Q. Peng, J. Guo, Q. Zhang, J. Xiang, B. Liu, A. Zhou, R. Liu, Y. Tian, *J. Am. Chem. Soc.* **2014**, *136*, 4113 – 4116.

Manuscript received: January 15, 2021
Revised manuscript received: March 24, 2021
Accepted manuscript online: May 11, 2021
Version of record online: June 9, 2021

